

# Topological Fluctuations in Dense Matter with Two Colors

Simon Hands and Philip Kenny

*Department of Physics, College of Science, Swansea University,  
Singleton Park, Swansea SA2 8PP, UK*

**Abstract:** We study the topological charge fluctuations of an  $SU(2)$  lattice gauge theory containing both  $N_f = 2$  and 4 flavors of Wilson fermion, at low temperature with non-zero chemical potential  $\mu$ . The topological susceptibility,  $\chi_T$ , is used to characterize differing physical regimes as  $\mu$  is varied between the onset of matter at  $\mu_o$  and color deconfinement at  $\mu_d$ . Suppression of instantons by matter via Debye screening is also investigated, revealing effects not captured by perturbative predictions. In particular, the breaking of scale invariance leads to the mean instanton size  $\bar{\rho}$  becoming  $\mu$ -dependent in the regime between onset and deconfinement, with a scaling  $\bar{\rho} \propto \mu^{-2}$  over the range  $\mu_o < \mu < \mu_d$ , resulting in an enhancement of  $\chi_T$  immediately above onset.

## 1 Introduction

Lattice studies of matter at non-zero baryon density are hampered by the ‘sign problem’, which arises when a quark chemical potential term  $\mu$  is included in the Euclidean QCD action. The resulting complex nature of the fermion determinant precludes a positive definite probability measure and computational techniques based on importance sampling break down. A gauge theory which is accessible to Monte Carlo simulations is  $QC_2D$ , based on gauge group  $SU(2)$ , describing “two color matter”. In  $QC_2D$ , quarks belong in the pseudoreal  $\mathbf{2}$  representation of  $SU(2)$  which can guarantee a positive definite measure.

Studies of two color matter have been performed utilising a number of fermion formulations. The series of works obtained from simulations involving two and four flavors of Wilson fermion [1, 2, 3] have revealed a scenario in which, as  $\mu$  is increased, baryonic matter forms at an onset  $\mu_o = m_\pi/2$  whereupon the matter then exists in a superfluid state with a progression from a dilute gas of tightly-bound diquark pairs to degenerate quark matter, culminating in color deconfinement at around  $\mu \approx 1.1m_\pi$ . This Letter supplements this picture with an investigation of topological effects observed on the same lattice configurations.

The topological charge density  $q_T$  may be defined in terms of the Yang-Mills field tensor as

$$q_T = \frac{1}{32\pi^2} F_{\mu\nu} \tilde{F}_{\mu\nu} \quad (1)$$

with  $\tilde{F}_{\mu\nu} = \frac{1}{2}\epsilon_{\mu\nu\rho\sigma}F_{\rho\sigma}$ . The action is minimised when the condition  $F_{\mu\nu} = \pm\tilde{F}_{\mu\nu}$  is satisfied. The observable measured to study topological charge fluctuations is the *topological*

susceptibility,  $\chi_T$ , defined as

$$\chi_T = \frac{\langle Q^2 \rangle}{V}, \quad (2)$$

where  $Q = \int d^4x q_T$  and  $V = \int d^4x$ . Using large- $N_c$  methods  $\chi_T$  is estimated by means of the Witten-Veneziano formula [4, 5]

$$\chi_T = \frac{f_\pi^2}{2N_f} (m_\pi^2 + m_{\eta'}^2 - 2m_K^2) \quad (3)$$

to be  $(180 \text{ MeV})^4$  in the SU(3) gauge vacuum. Simulations of hot two color matter with two flavors of staggered quark (equivalent to  $N_f = 8$  continuum quark flavors) have shown this quantity drops sharply at the deconfining temperature and have suggested this also happens at non-zero chemical potential [6, 7]. When  $\chi_T$  is measured as a function of  $a\mu$ , the susceptibility remains constant before dropping dramatically at a critical chemical potential corresponding to both deconfinement and chiral symmetry restoration.

In a semi-classical picture topological charge is localised on four-dimensional objects called instantons, which are solutions of the self-dual condition for a local minimum of the action [8]. Another observable of interest is the size of an instanton  $\rho$ . This is a measure of the extent to which the gauge field action is localised. For classical Yang-Mills instantons the size may be considered arbitrary due to scale invariance and so  $\rho$  does not depend upon the action, and vice versa. However, in the quantum vacuum scale invariance is broken, and the typical size of an instanton is estimated to be in the region of 0.3 fm [9, 10].

In dense matter, Debye screening of color charge leads to instanton suppression [12]. Perturbative calculations [13] predict that instanton number at large chemical potential should go like

$$n(\mu) = n(\mu = 0) \exp(-N_f(\rho\mu)^2). \quad (4)$$

Therefore, as the number of quark flavors  $N_f$  is increased, instantons should be suppressed and  $\chi_T$  should decrease. It should also be expected that, if the average instanton size  $\rho$  is indeed fixed, then the extra matter present as  $\mu$  is increased will screen the topological charge and suppress  $\chi_T$  still further.

## 2 Methodology

In order to explore instanton effects on a lattice we replace the continuum topological charge density  $q_T$  (1) with its lattice counterpart

$$q_L(x) = \frac{1}{32\pi^2} \epsilon_{\mu\nu\rho\sigma} \text{Tr}(U_{\mu\nu}(x)U_{\rho\sigma}(x)) \quad (5)$$

where  $U_{\mu\nu}(x)$  is the product of link variables around a plaquette at site  $x$  in the  $\mu - \nu$  plane [14]. The charge density is thus measured by taking the trace of the product of

two orthogonal plaquettes. The total charge  $Q_L$  is obtained via  $Q_L = \sum_x q_L(x)$ . Within each configuration, the peaks due to the presence of instantons (whose structure may extend over a scale  $\rho \gg a$ , where  $a$  is the lattice spacing) are mutated by short scale ( $\mathcal{O}(a)$ ) fluctuations. Such UV fluctuations are highly undesirable as they contribute to the total charge but obscure the ‘real’ instantons, and so the measured susceptibility can be an overestimate [15]. The lattice topological susceptibility  $\chi_L \equiv \langle Q_L^2 \rangle / V$  differs from the continuum value by both a multiplicative factor  $Z$  and an additive one  $M$ :

$$\chi_L = Z^2 a^4 \chi_T + M. \quad (6)$$

$Z$  and  $M$  depend on several factors including the quark mass, the inverse coupling  $\beta$  and the choice of fermion operator [7]. In general, on the lattice,  $Z \neq 1$  and the charge  $Q_L$  is not integer-valued. The challenge is to minimise the unwanted, short distance contributions while in the process recovering the continuum value in an unambiguous fashion.

$Q_L$  for a given configuration of gauge fields is calculated by means of Eqn. (5). The effects of UV fluctuations are minimised by cooling [16], whereby a new configuration is generated from the old by visiting lattice sites in turn and minimising the action locally. Repeating this succesively has the effect of smoothing out fluctuations and revealing the underlying topological structure in the gauge fields. By prudent use of cooling, the multiplicative factor  $Z \rightarrow 1$  as the unwanted fluctuations are eliminated. However, excessive cooling eliminates not just the UV fluctuations but will also shrink and ultimately eradicate the ‘real’ instantons. If cooling shrinks an instanton until its size  $\rho < a$  then it ‘falls through’ the lattice and some of the topological information is lost. If only larger instantons contribute to the total charge then there is a tendency to underestimate  $Q_T$ . Information can also be lost as too much cooling has a tendency to annihilate instanton – anti-instanton pairs. The total charge may remain the same but the charge density is reduced. Therefore, it is vital that good control of the cooling process is maintained.

The additive constant  $M$  may be dealt with by equating it to the value of the topological susceptibility in the  $Q_T = 0$  sector, setting  $M = \chi_0 \equiv \chi_T(Q = 0)$ . As we have no prior knowledge to suggest that our ensemble is in the trivial sector we must modify Eqn. (2). In the non-trivial sector  $M$  can be eradicated by redefining

$$a^4 \chi_T = \frac{\langle Q^2 \rangle - \langle Q \rangle^2}{V} \quad (7)$$

Thus, by measuring the charges on a number of cooled field configurations with  $Z \sim 1$  and calculating  $\chi_T$  by means of (7), the physical topological susceptibility can be extracted from the lattice one. Henceforth, we discard the references to lattice values via our subscripts  $L$  and merely label  $\chi$  and  $Q$  with the subscript  $T$ .

The cooling method employed here uses a computer program to read the gauge field information from each configuration and then calculate the total action by summing over the plaquettes. In general, this is not the minimum action. A point is then chosen and

a link variable  $U_\mu(x)$  is selected. There are 6 plaquettes with this link in common. The code sums the link products, in the form of unitary matrices which form the ‘staples’ bordering the link  $U_\mu(x)$ , resulting in a  $2 \times 2$  matrix  $V$ . The matrix  $V$  is non-unitary and must be renormalised as  $\tilde{V} = (\text{Det } V)^{-1/2}V$ . Keeping  $\tilde{V}$  fixed, the action is then minimised by modifying  $U_\mu(x)$ . By systematically working through the old configuration and updating all links  $U_\mu(x)$  a new configuration is produced with a lower action than the original one. This completes the first cooling sweep. By predetermining the number of sweeps to be performed, the process repeats automatically and the configuration is cooled to the required extent. When cooling is complete, the code then searches through the final configuration to find where the peaks of the action are located and  $F\tilde{F}$  at these points is recorded. Setting a minimum cutoff for  $F\tilde{F}$  allows the code to disregard the smallest fluctuations. Imposing a second cutoff for the maximum extent of the gauge fields inside an instanton minimizes any finite volume effects associated with excessively large instantons. Once the required topological information is extracted from the cooled configuration, the program then moves onto the next configuration in the ensemble and repeats as necessary.

To find the total topological charge on each configuration, a second program obtains the net value of all the peaks of  $F\tilde{F}$  from the output of the first, providing a sequence of estimates for the fluctuating variable  $Q_T$ . The topological susceptibility is estimated from this using Eqn.(7).

One aspect of topological structure that is worth investigating is the size distribution of the instantons. Instanton size may be calculated from the peak value of the topological charge density using

$$q_{\text{peak}} = \frac{6}{\pi^2 \rho^4}. \quad (8)$$

This classical approximation works reasonably well for large lattice instantons, but for smaller ones whose size is of the order of the lattice spacing, corrections of  $\mathcal{O}(a^2)$  are needed. The necessary correction factors for  $N_c = 3$  were calculated by Smith and Teper by cooling a classical instanton and then parametrising the resulting relationship between  $Q$  and  $\rho$  [15]. The computational method employed in this study involved reading the peak values of the charge from the lattice configurations and then applying iterative bisection to find a value for  $\rho$  which satisfied Eqn. (8) to within a predetermined error factor  $\epsilon$ .

### 3 Numerical Results

Information about the topological structure was extracted using two different gauge field ensembles. The first was generated on a  $12^3 \times 24$  lattice with  $\sqrt{\sigma a} = 0.415(18)$  ( $\sigma$  is the string tension) using  $N_f = 2$  flavors of Wilson fermion at an inverse coupling  $\beta = 1.9$  [2]. The fermion action included a diquark source term  $aj = 0.04$  and the value of the hopping parameter  $\kappa = 0.168$ . The second ensemble was generated on the same system size,  $\beta$  and  $j$  using  $N_f = 4$ , resulting in a significantly finer lattice with

$\sqrt{\sigma}a = 0.138(4)$  [3]. This time  $\kappa$  was chosen to be 0.158; both ensembles therefore had a matched pion mass  $m_\pi a = 0.68(1)$ . Although we choose to plot several figures in cutoff units  $\mu a$ , the horizontal axis could therefore equally be regarded as being calibrated in units of  $\mu/m_\pi$ , as noted in [3]. In both cases chemical potential was introduced via the standard Hasenfratz-Karsch prescription [18]. The minimum cutoff for  $F\tilde{F}$  was  $q_{cut} = 0.02a^{-4}$  whereas any instantons larger than one third of the spatial extent of the lattice were ignored.

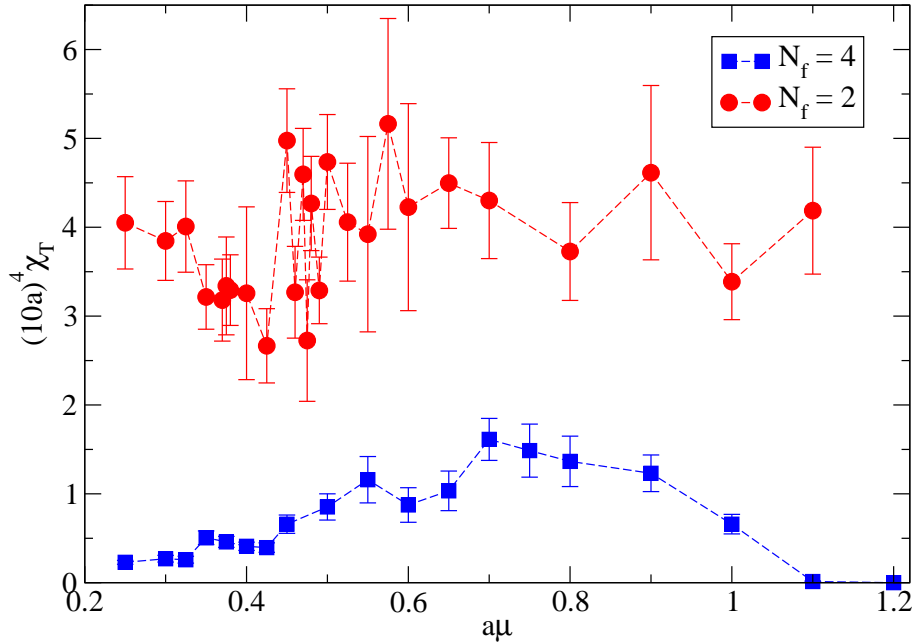


Figure 1: *Topological susceptibility  $a^4\chi_T$  versus chemical potential for  $N_f = 2$  and  $N_f = 4$  performing 10 cooling steps.*

The topological susceptibility of the  $N_f = 2$  and 4 configurations was measured across a range  $\sim 0.25 \leq a\mu \leq 1.1$ . Fig. 1 shows the behaviour of  $\chi_T$  for both theories. In order to verify the validity of our approach to cooling, the same ensemble was submitted to both 10 and 20 cooling steps. As the extra cooling had little effect on the signal, we are confident we are characterising the underlying topology satisfactorily.

In the  $N_f = 2$  case the signal remains fairly consistent across the range studied. There are possible signs of some minor downward fluctuations at  $a\mu \sim 0.4$  and  $a\mu \sim 0.5$ , but beyond  $a\mu = 0.5$  the data remains flat. The  $N_f = 4$  data obtained on a finer lattice are more interesting. Fig. 1 suggests that the extra flavors have suppressed the instantons with the peak value of  $\chi_T^{N_f=4} \sim 0.5\chi_T^{N_f=2}$ . Moreover, the suppression of  $\chi_T^{N_f=4}$  at the lowest densities is much greater can be explained purely by a change in  $N_f$ , and its behaviour with increasing  $\mu$  is not as expected if the relation in Eqn.(4) is correct (and assuming  $\rho$  to be independent of  $N_f$ );  $\chi(\mu)$  initially increases instead of being suppressed.

At larger densities the situation changes. A comparison of  $\chi_T^{N_f=4}$  with the Polyakov

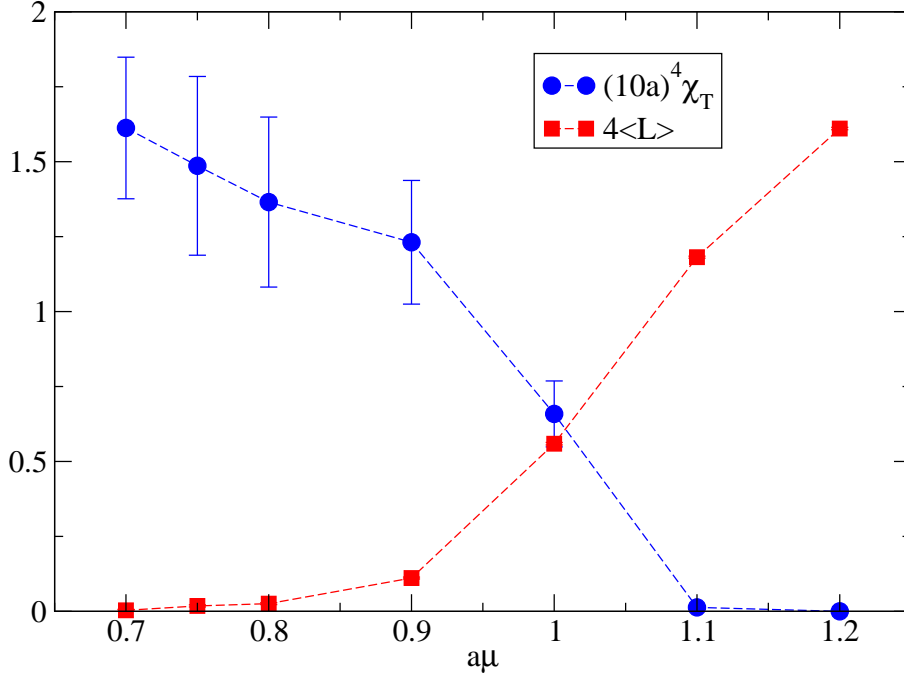


Figure 2: The suppression of  $\chi_T$  coinciding with the rise in  $\langle L \rangle$  for  $N_f = 4$ . Note  $\langle L \rangle$  has been rescaled for clarity.

loop  $\langle L \rangle$  from [3] over the range  $0.7 < a\mu < 1.2$  is shown in Fig. 2. It illustrates nicely how the fall in  $\chi_T$  coincides with the rise in  $\langle L \rangle$ . The Polyakov loop begins to rise from zero at  $a\mu \approx 0.8$ , whereas  $\chi_T$  starts to fall noticeably just a little later at  $a\mu \approx 0.9$ . Ref. [3] identified a “deconfining” value of chemical potential  $a\mu_d \approx 0.75$  based on the behaviour of  $\langle L \rangle$ ; Fig. 2 suggests deconfinement in dense matter is accompanied by suppression of topological fluctuations.

It is worth noting that although effort has been made to make a direct comparison of the  $N_f = 2$  and  $N_f = 4$  data sets, in reality they are distinct theories. When comparing both ensembles it is important to remember that the physical volumes (ie. as measured in string tension units) of the two lattices differ by a factor of  $\sim 3^4$ . Hence it is difficult to make any useful quantitative comparison of  $\chi_T$  for the two theories directly. It is more useful to rescale  $\chi_T$  in each case as some dimensionless parameter and then make a comparison of the two. Fig. 3 shows the topological susceptibility rescaled and plotted as the fourth root of  $a^4 \chi_T$  divided by the square root of the string tension  $a^2 \sigma$ . From this it is possible to compare the results to (3), which implies  $\chi_T^{1/4} = 180$  MeV. For  $N_f = 2$ ,  $\chi_T^{1/4}/\sigma^{1/2} = 0.3493 \pm 0.0076$ , and for  $N_f = 4$ ,  $\chi_T^{1/4}/\sigma^{1/2} = 0.4837 \pm 0.0198$ . Assuming  $\sigma = (440\text{MeV})^2$  leads to

$$\chi_T^{\frac{1}{4}} = \begin{cases} 156 \pm 3\text{MeV} & N_f = 2; \\ 213 \pm 9\text{MeV} & N_f = 4. \end{cases} \quad (9)$$

Both results are in the range suggested by the Witten-Veneziano formula. That the

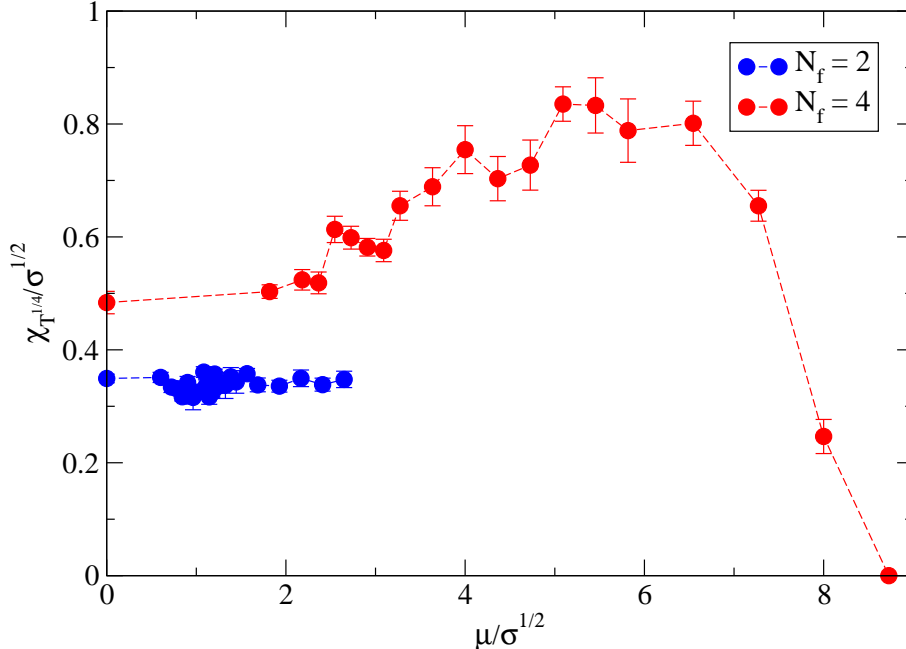


Figure 3: The dimensionless quantity  $\chi_T^{1/4}/\sigma^{1/2}$  versus  $\mu/\sigma^{1/2}$  for 2 and 4 flavors.

value for  $N_f = 2$  is smaller than the  $N_f = 4$  value by about 25% hints that much of the topological information is being missed due to the coarseness of the lattice.

The instanton size distribution was plotted for both the two and four flavor configurations. To compensate for inequalities in the sizes of the data sets, each distribution curve is normalized, keeping the area under the curve consistent. Using the same scale determination that led to Eqn. (9), for  $N_f = 2$  (see Fig. 4) at  $a\mu = 0.25$ , the majority lay within the range  $0.18 \leq \rho \leq 0.5\text{fm}$ , with the average size being  $\bar{\rho} \sim 0.28\text{fm}$ . This compares well with the phenomenologically derived value  $\bar{\rho} \approx 0.3 \text{ fm}$  [17]. The sharp cutoff at  $\rho = a$  is where instantons smaller than this ‘fall through’ the lattice and do not contribute. Similar distribution curves are also plotted for higher values of  $\mu$  to see if there is any effect with increasing density. While there is a hint that larger instantons are slightly suppressed at larger  $\mu$ , no significant  $\mu$ -dependence is observed and all the curves are qualitatively the same.

By contrast, Fig. 5 shows how the instanton size distribution evolves with  $\mu$  for  $N_f = 4$ . At  $a\mu = 0.25$  the distribution is fairly uniform. As  $\mu$  increases the number of large instantons falls as that of smaller-sized instantons rises, and the distribution becomes taller and narrower, with a peak at  $a\mu = 0.9$  of  $\bar{\rho} \sim 1.4\text{fm}$ . For  $a\mu = 1.0$  the curve has rapidly flattened and has a very similar profile to that for  $a\mu = 0.45$ . The prevalence of small-sized instantons drives down the average instanton size. The cutoff at large  $\rho$  for  $a\mu = 0.25, 0.45$  results from the constraint on the maximum possible instanton size. Such a filter on  $\rho$  is needed to minimize finite volume effects and to prevent instantons overlapping one another. As  $\mu$  increases,  $\bar{\rho}$  decreases and this becomes

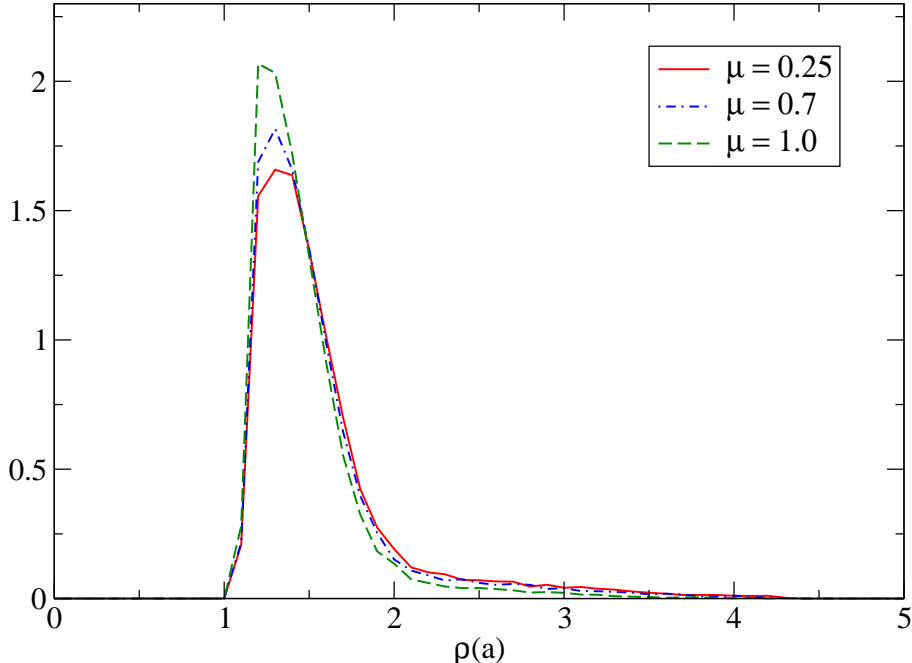


Figure 4: Normalized instanton size distribution at three different chemical potentials for  $N_f = 2$ . The average size  $\bar{\rho} \simeq 0.3$  fm.

less of an issue but at low  $\mu$ , where there is a greater number of large-sized instantons, it seems likely that some topological information is lost due to the IR cutoff.

When  $\bar{\rho}$  is plotted as a function of  $\mu$  (see Fig. 6) it is apparent that the  $N_f = 4$  instantons are shrinking between onset and deconfinement, after which there is a sharp rise in size. This rise coincides with the rapid flattening of the  $a\mu = 1.0$  distribution curve recorded in Fig. 5. In the range  $\mu_o < \mu < \mu_d$ , empirically  $\bar{\rho} \propto \mu^{-2}$  and this behaviour is plotted along with the data. This contrasts markedly with the  $N_f = 2$  data, where  $\rho$  appears to be almost  $\mu$ -independent. At most there is a very gentle monotonic fall in  $\bar{\rho}$  for  $\mu > \mu_o$ . A consideration of the behaviour of the size distribution in Fig. 5 suggests why that might be. The most significant  $\mu$ -dependent effects are seen for small-sized instantons with  $\rho < 3a^{N_f=4} \approx a^{N_f=2}$ . Thus, the  $N_f = 2$  lattice may well be too coarse for this detail to be seen.

It is also of interest to compare the behaviour of  $\rho(\mu)$  for  $N_f = 4$  with the predictions of thermal field theory. The perturbative result (4) of [13] implies that, for constant  $\rho$   $n$  is suppressed by a factor  $e^{-N_f \rho^2 \mu^2}$  as density is increased. Thus,  $\chi_T$  should be suppressed by increasing  $\mu$ . In Fig. 1  $\chi_T^{N_f=4}$  rises as  $\mu$  increases, which seems to be incompatible with the perturbative result. However, if we take into account the non-perturbative information on  $\rho(\mu) \propto \mu^{-2}$  in Eqn.(4) we find

$$n(\mu) \propto \exp(-N_f(\rho(\mu)\mu)^2) = A \exp\left(-\frac{B}{\mu^2}\right). \quad (10)$$



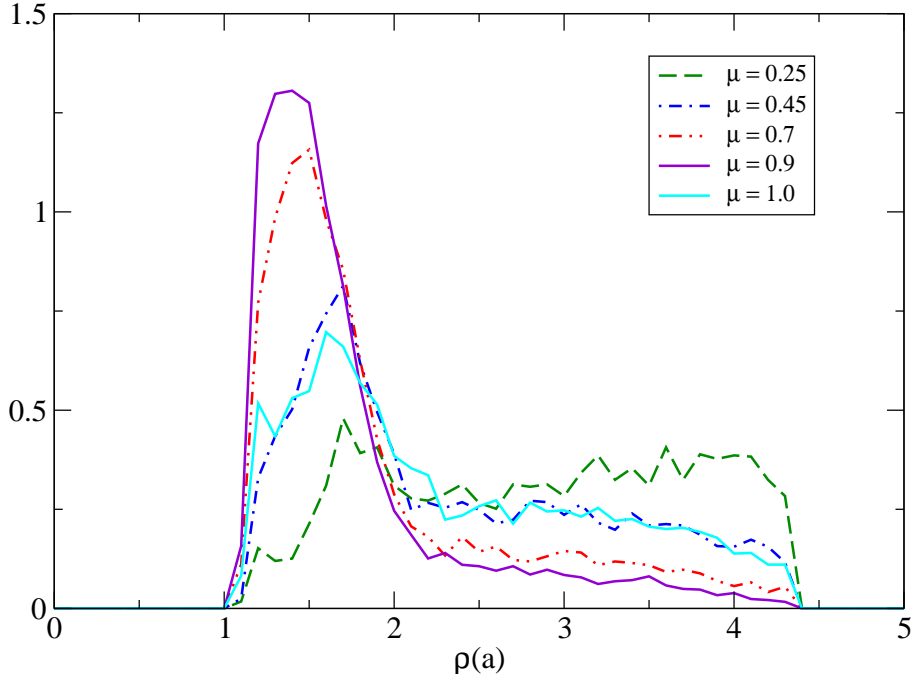


Figure 5: *Behaviour of the normalized  $N_f = 4$  instanton size distribution at various  $\mu$  values.*

The parameter  $A$  includes  $n(\mu = T = 0)$  plus thermal contributions due to the fact that we are working at low but non-zero  $T$ . The parameter  $B$  includes the constant of proportionality for instanton size as a function of  $\mu$  multiplied by a factor of  $N_f$ . When a function of this form is plotted along with  $\chi_T^{N_f=4}$  in Fig. 7 in the range  $\mu_o < \mu < \mu_d$  we see a fair correspondence between the two. The best fit is found with  $A = 1.8255$  and  $B = 0.2231$ . This suggests that the enhanced topological fluctuations observed in baryonic matter at moderate density are a direct result of the  $\mu$ -dependence of the instanton scale size.

## 4 Conclusion

In this Letter we have presented the first exploratory study of topological fluctuations of non-abelian gauge fields in cold dense baryonic matter, using ensembles generated for a range of  $\mu$  with both  $N_f = 2$  and  $N_f = 4$ .

For  $N_f = 2$  the topological susceptibility remained flat across the whole range studied. It is likely that the lattice is too coarse to be able to capture the topological detail adequately. The fact that for the two flavor ensemble  $\chi_T$  was measured to be  $\chi_T \simeq (150 \text{ MeV})^4$  suggests that a lot of topological information is falling through the lattice and being lost.

With an increase in the number of flavors to  $N_f = 4$ , the resulting finer lattice was

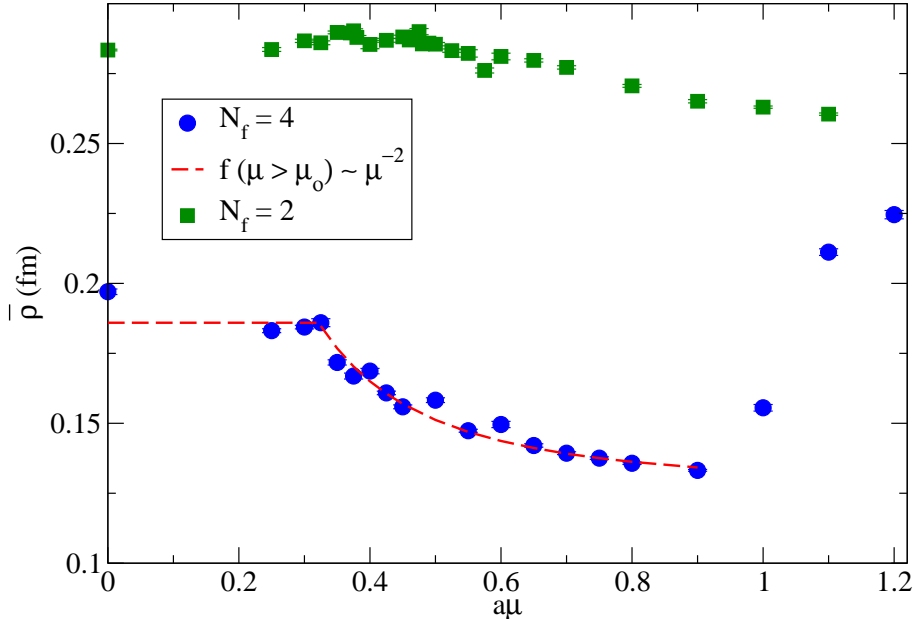


Figure 6: Average instanton size versus chemical potential for  $N_f = 2$  and for  $N_f = 4$  fitted with function  $f(\mu) \propto \mu^{-2}$  for  $\mu_o < \mu < \mu_d$ .

able to expose more detail about the distribution of instanton size and its evolution with  $\mu$ . Once chemical potential is increased beyond onset, the instanton size becomes density-dependent. The large instantons found at low  $\mu$  are suppressed as  $\mu$  is increased, driving down the average size to a minimum of  $\bar{\rho} \sim 0.14$  fm at around  $a\mu \sim 0.9$ . The smaller instantons result in reduction in screening of topological charge fluctuations, so that the topological susceptibility  $\chi_T$  initially rises for  $\mu \geq \mu_o$ . In the deconfined phase  $\mu \geq \mu_d$ , however, the average instanton size rises sharply, and  $\chi_T$  is suppressed.

While it is tempting to ascribe the differences observed between  $N_f = 2$  and  $N_f = 4$  entirely to the different lattice spacings, as measured in string tension units, we should remain mindful that they are two different theories; in particular the thermodynamics studies of [2, 3] reveal that for  $N_f = 2$  the regime just above onset is weakly-interacting and dilute, apparently well-described as a non-relativistic Bose gas of tightly-bound scalar diquarks. By contrast, matter with  $N_f = 4$  appears relativistic and strongly-interacting for all  $\mu \geq \mu_o$ . A systematic study of the  $\mu$ -dependence of topological fluctuations in QC<sub>2</sub>D, therefore, must await the generation of gauge ensembles on a finer lattice.

## Acknowledgments

This project was enabled with the assistance of IBM Deep Computing. We are grateful to Biagio Lucini and Jon-Ivar Skullerud for their help and advice. We have also enjoyed

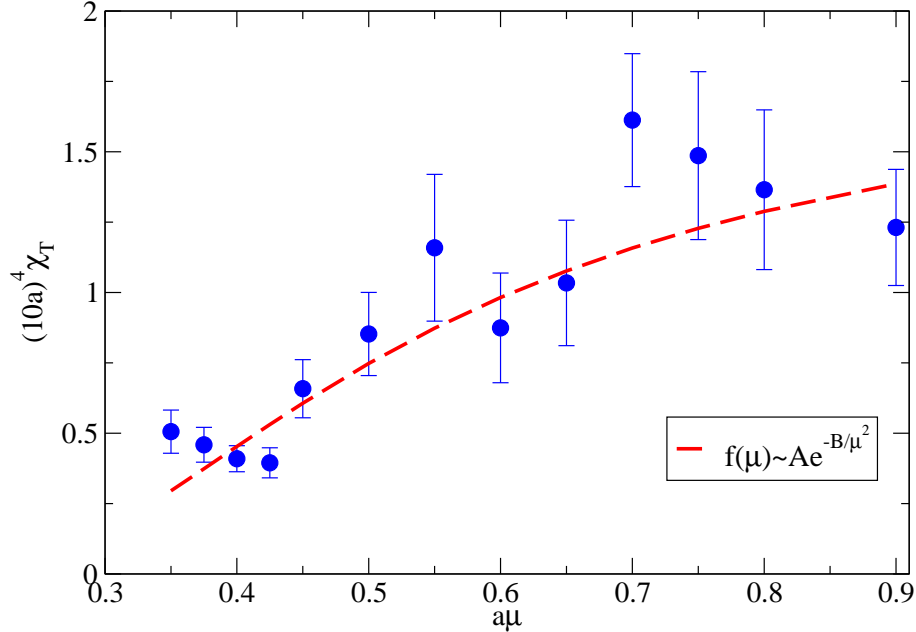


Figure 7:  $\chi_T(\mu)^{N_f=4}$  for  $\mu \in (\mu_o, \mu_d)$ , along with a fit to  $f = A \exp(-B/\mu^2)$ .

discussing our results with Massimo D’Elia and Ernst-Michael Ilgenfritz.

## References

- [1] S. Hands, S. Kim and J.I. Skullerud, *Eur. Phys. J. C* **48** (2006) 193.
- [2] S. Hands, S. Kim and J.I. Skullerud, *Phys. Rev. D* **81** (2010) 091502(R).
- [3] S. Hands, P. Kenny, S. Kim and J.I. Skullerud, arXiv:hep-lat/1101.4961
- [4] E. Witten, *Nucl. Phys. B* **156** (1979) 269.
- [5] G. Veneziano, *Nucl. Phys. B* **159** (1979) 213-224.
- [6] B. Alles, and M. D’Elia, in *A Sense of Beauty in Physics*, p. 123, eds. M. D’Elia *et al* (Pisa University Press 2006), arXiv:hep-lat/0602032
- [7] B. Alles, M. D’Elia, and M.P. Lombardo, *Nucl. Phys. B* **752** (2006) 124.
- [8] A.A. Belavin, A.M. Polyakov, A.S. Shvarts, and Y.S. Tyupkin, *Phys. Lett. B* **59**, 85-87 (1975).
- [9] M.A. Shifman, A.I. Vainshtein, and V.I. Zakharov, *Phys. Lett. B* **76**, 471 (1978).
- [10] E.V. Shuryak, *Nucl. Phys. B* **198**, 83 (1982).

- [11] C. Michael, and P.S. Spencer, Phys. Rev. D **52**, 4691-4699 (1995).
- [12] T. Schafer, Phys. Rev. D **57**, 3950-3961 (1998).
- [13] E.V. Shuryak, Nucl. Phys. B **203**, 140 (1982).
- [14] P. DiVecchia, K. Fabricius, G.C. Rossi, and G. Veneziano, Nucl. Phys. B **192** (1981) 392.
- [15] D.A. Smith, and M.J. Teper, Phys. Rev. D **58** (1998) 014505.
- [16] M.J. Teper, Phys. Lett. B **162**, 357 (1985).
- [17] E.V. Shuryak, and T. Schafer, Ann. Rev. Nucl. Part. Sci. Vol **47**, 359-394 (1997).
- [18] P. Hasenfratz and F. Karsch, Phys. Lett. B **125** (1983) 308.